Anterior Segment Dysgenesis and Early-Onset Glaucoma in *nee* Mice with Mutation of *Sh3pxd2b*

Mao Mao,[1] *Adam Hedberg-Buenz,*[1] *Demelza Koehn,*[1] *Simon W. M. John,*[2] *and Michael G. Anderson*[1,3]

Purpose. Mutations in *SH3PXD2B* cause Frank-Ter Haar syndrome, a rare condition characterized by congenital glaucoma, as well as craniofacial, skeletal, and cardiac anomalies. The *nee* strain of mice carries a spontaneously arising mutation in *Sh3pxd2b*. The purpose of this study was to test whether *nee* mice develop glaucoma.

Methods. Eyes of *nee* mutants and strain-matched controls were comparatively analyzed at multiple ages by slit lamp examination, intraocular pressure recording, and histologic analysis. Cross sections of the optic nerve were analyzed to confirm glaucomatous progression.

Results. Slit lamp examination showed that, from an early age, *nee* mice uniformly exhibited severe iridocorneal adhesions around the entire circumference of the eye. Presumably as a consequence of aqueous humor outflow blockage, they rapidly developed multiple indices of glaucoma. By 3 to 4 months of age, they exhibited high intraocular pressure (30.8 ± 12.5 mm Hg; mean ± SD), corneal opacity, and enlarged anterior chambers. Although histologic analyses at P17 did not reveal any indices of damage, similar analysis at 3 to 4 months of age revealed a course of progressive retinal ganglion cell loss, optic nerve head excavation, and axon loss.

Conclusions. Eyes of *nee* mice exhibit anterior segment dysgenesis and early-onset glaucoma. Because SH3PXD2B is predicted to be a podosome adaptor protein, these findings implicate podosomes in normal development of the iridocorneal angle and the genes influencing podosomes as candidates in glaucoma. Because of the early-onset, high-penetrance glaucoma, *nee* mice offer many potential advantages as a new mouse model of the disease. (*Invest Ophthalmol Vis Sci.* 2011; 52:2679–2688) DOI:10.1167/iovs.10-5993

The glaucomas are a collection of ocular diseases involving degeneration of retinal ganglion cells, excavation of the optic nerve head, and progressive loss of vision. Forms of glaucoma affect approximately 60 million people worldwide.[1,2] Elevated intraocular pressure (IOP) is a risk factor and is currently the only clinically treatable feature.[3,4] Many of the factors that precipitate elevations in IOP remain to be identified, as do the molecular pathways that underlie additional risk factors. One means of filling this gap in our knowledge is through genetics. While many of the most common forms of glaucoma appear to be sporadic and are presumably genetically complex, several Mendelian-acting mutations have been identified.[5,6] Glaucoma can also occur as a component of several broader syndromes for which causative mutations have been identified. These include Axenfeld-Rieger syndrome,[7] nail-patella syndrome,[8] Weill-Marchesani syndrome,[9] Charcot-Marie-Tooth disease,[10] and others. With the identification of each of these glaucoma-causing genes, there has been a corresponding new opportunity for discovering molecular pathways and potential therapeutic targets relevant to glaucoma.

One of the most recent additions to the list of glaucoma-causing genes resulted from studies of Frank-Ter Haar syndrome, a rare disorder involving congenital glaucoma as well as craniofacial, skeletal, and cardiac anomalies.[11,12] Homozygosity mapping in patients from 12 families established that mutations disrupting *SH3PXD2B* cause Frank-Ter Haar syndrome.[13] The SH3PXD2B protein (commonly referred to as TKS4) is an adaptor protein that contains an N-terminal PX domain, four SH3 domains, multiple PXXP motifs, and several tyrosine phosphorylation sites.[14,15] In *Src*-transformed murine fibroblasts, SH3PXD2B is essential for the formation of podosomes,[15] adhesive structures that bind the cell to the extracellular matrix and have matrix-degrading activity.[16] In vivo, podosomes have been observed in a variety of tissues, notably including cells of the trabecular meshwork in the eye.[17] Thus, these observations suggest that SH3PXD2B is most likely important for modulating an extracellular matrix that is essential in the development or function of the eye. Precisely how SH3PXD2B contributes to the form of congenital glaucoma that is present in Frank-Ter Haar syndrome remains unknown.

Recently, two mouse models with potential value in investigating the functions of SH3PXD2B have been described. The spontaneous *nee* mutation contains a 1-bp deletion in the last exon of the *Sh3pxd2b* gene that is predicted to lead to the production of a truncated protein in which a portion of the third and entirety of the fourth SH3 domains are deleted.[18] We have previously reported that by 1 month of age, B10-*Sh3pxd2b*^{nee} mice exhibit a form of anterior segment dysgenesis characterized by peripheral iridocorneal adhesions, enlarged anterior chambers, and corneal opacity.[18] These phenotypes are all likely indices of glaucoma secondary to anterior segment dysgenesis. In addition, Iqbal et al.[13] have recently described many phenotypic similarities and elevated IOP in a *Sh3pxd2b* mutant strain generated by gene trap.[13] In this study, we extended the knowledge of SH3PXD2B-mediated phenotypes by examining B10-*Sh3pxd2b*^{nee} mice at multiple ages and testing whether optic nerves of these mice are indeed damaged by glaucoma. The B10-*Sh3pxd2b*^{nee} mice exhibited drastically elevated IOP and early degeneration of the optic nerve. Thus, B10-*Sh3pxd2b*^{nee} mice represent a new

From the Departments of [1]Molecular Physiology and Biophysics and [3]Ophthalmology and Visual Sciences, The University of Iowa, Iowa City, Iowa; and the [2]Howard Hughes Medical Institute, The Jackson Laboratory, Bar Harbor, Maine.

Supported by National Eye Institute Grants EY11721 (SWMJ) and EY017673 (MGA). SWMJ is an Investigator of The Howard Hughes Medical Institute.

Submitted for publication June 2, 2010; revised October 8, 2010; accepted November 3, 2010.

Disclosure: **M. Mao**, None; **A. Hedberg-Buenz**, None; **D. Koehn**, None; **S.W.M. John**, None; **M.G. Anderson**, None

Corresponding author: Michael G. Anderson, Department of Molecular Physiology and Biophysics, 6-430 Bowen Science Building, 51 Newton Road, Iowa City, IA 52242; michael-g-anderson@uiowa.edu.

mouse model of glaucoma and, by extension, implicate a new pathway of candidates likely to affect the eye in health and disease.

METHODS

Animal Husbandry and Genotyping

All mice were obtained from The Jackson Laboratory (Bar Harbor, ME). Experiments measuring IOP were performed at The Jackson Laboratory, where the mice were housed in cages containing white pine bedding and were maintained on a 6% fat NIH 31 diet provided ad libitum with water acidified to pH 2.8 to 3.2 in an environment was kept at 21°C, with a 14-hour light:10-hour dark cycle. All other experiments were performed at The University of Iowa, where the mice were housed in cages containing dry bedding (Cellu-dri; Shepherd Specialty Papers, Kalamazoo, MI) and maintained on a 4% fat NIH 31 diet provided ad libitum. The environment was kept at 21°C, with a 12-hour light:12-hour dark cycle. The *Sh3pxd2b*^{nee} mutation was studied in the genetic background in which it arose, B10.A-*H2*^{b4}/(4R)SgDvEgJ mice (abbreviated throughout as B10-*Sh3pxd2b*^{nee}). The presence of the *nee* mutation was genotyped by assaying for the absence or presence of an *Rsa*I restriction enzyme site that is abolished by the *nee* mutation,[18] and the stock was maintained in heterozygote × heterozygote crosses. All mutant mice analyzed were homozygous for the *nee* mutation, with littermates homozygous for the wild-type allele serving as controls. All animals were treated in accordance with the ARVO Statement for the Use of Animals in Ophthalmic and Vision Research. All experimental protocols were approved by the Animal Care and Use Committee of The University of Iowa.

Slit Lamp Examination

Anterior chamber phenotypes were assessed with a slit lamp (SL-D7; Topcon, Tokyo, Japan) and photodocumented with a digital camera (D100; Nikon, Tokyo, Japan). With the exception of Supplementary Figures S3C and S3D (http://www.iovs.org/lookup/suppl/doi:10.1167/iovs.10-5993/-/DCSupplemental), which are presented with less image reduction, all images were taken using identical camera settings and prepared by processing with identical image software. All ocular examinations were performed on conscious mice.

CCT Measurement

An ultrasound pachymeter (Corneo-Gage Plus; Sonogage, Cleveland, OH) was used to measure murine CCT.[19] Probe movements were controlled with a micromanipulator placed under a dissecting microscope, with the probe and central cornea aligned perpendicular to each other. The mice were anesthetized with a mixture of ketamine (100 mg/kg) and xylazine (10 mg/kg). Balanced salt solution (BSS; Alcon Laboratories, Inc., Fort Worth, TX) was applied to the eye to maintain a consistent tear film.

Light Microscopy of Dissected Lenses

The enucleated eyes were immediately placed into glass Petri dishes containing prewarmed (37°C) PBS (pH 7.4). The lenses were removed and transferred to new glass Petri dishes containing fresh prewarmed PBS, placed under a light microscope (BX52; Olympus, Tokyo, Japan) equipped with a digital camera (DP70; Olympus, Tokyo, Japan), and photographed in two separate conditions. First, lenses were viewed in dark field and photographed with identical microscope settings. In these images, exposure times varied, to enable visualization of lenses with more severe opacities. Lenses with mild or no opacities were photographed with a 4-μs exposure time, whereas lenses with more severe opacities required a 20-μs exposure time. Second, lenses were placed atop 200-mesh copper grids that were immersed at the bottom of the Petri dishes, viewed in bright field, and photographed with microscope and camera settings as were used in the first condition.

IOP Measurement

IOP was measured with a microneedle cannulation system, as previously described.[20] In brief, mice were anesthetized by intraperitoneal injection of a mixture of ketamine (100 mg/kg) and xylazine (9 mg/kg). After anesthesia, a microneedle was inserted via a micromanipulator into the anterior chamber, and pressure was recorded for 1 minute.

Histology

Eyes were fixed with zinc-formalin (Alcoholic Z-fix; Anatech, Battle Creek, MI) for 24 to 48 hours at room temperature. Eyes shown in Figures 2, 5, and 6 were subsequently rinsed with 0.1 M sodium cacodylate, postfixed with 1% osmium tetroxide, rinsed in buffer, and dehydrated with a graded series of acetone concentrations. After eyes were embedded in Eponate-12 resin, 1-μm sections were cut. Eye sections shown in Figure 3 were processed through a graded series of ethanol concentrations and subsequently infiltrated with embedding solution (JB-4; Electron Microscopy Sciences, Hatfield, PA) for 48 hours. Two-micrometer sagittal sections were then cut.

Cross-sections of the optic nerve were examined for glaucomatous damage by using a modified *para*-phenylenediamine (PPD) staining protocol.[21] In brief, heads in which the skull had been opened and most of the brain dissected to leave a thin layer of tissue covering the optic nerves were fixed overnight in half-strength Karnovsky's fixative (2.5% glutaraldehyde, 2% paraformaldehyde in 0.1 M sodium cacodylate). The following day, optic nerves were dissected from the skull and fixed in half-strength Karnovsky's fixative for an additional 24 hours. Nerves were subsequently rinsed with 0.1 M sodium cacodylate, postfixed with 1% osmium tetroxide, rinsed in buffer, and dehydrated with a graded series of acetone concentrations. After they were embedded in Eponate-12 resin, 1-μm sections were collected, stained with 1% PPD for 40 minutes, and imaged by light microscopy. The number of axons were assessed, as previously described.[22] In brief, axons from 12 nonoverlapping fields were counted at 1000× magnification. Fields were evenly spread throughout the cross-section of the nerve, with the total area of counted fields equaling 10% of the cross-sectional area of each nerve. The total number of axons for each nerve was estimated by multiplying the sum of the axons in the counted fields by 10.

Collection of Dissected Ocular Tissues from Mice

Freshly enucleated eyes were carefully dissected in PBS, and multiple ocular tissues were collected. Globes were cut along the limbus to separate the anterior/posterior segments and the lens removed. From the anterior segment, the iris was first removed with no. 5 forceps. Next, Vannas-style spring scissors were used to separate the cornea and the peripheral limbal ring. Because the trabecular meshwork was too small to dissect from the limbal ring, the entirety of the limbal ring, containing ocular drainage structures, ciliary body, cornea, and sclera, was used as a single tissue. From the posterior segment, the neural retina was removed, and a 0.5-cm segment of optic nerve immediately posterior to the globe was collected. After external muscles and connective tissues were removed, the remaining posterior globe was collected. Tissues from four C57BL/6J eyes were pooled per sample.

Reverse-Transcription PCR

Two-step reverse-transcription (RT)-PCR was performed as previously described.[23] Briefly, tissues were homogenized with plastic pestles, and total RNA was extracted, treated with DNase, and purified (Aurum Total RNA Mini Kit; Bio-Rad Laboratories, Hercules, CA). First-strand cDNA was synthesized from 100 μg total RNA (iScript cDNA Synthesis Kit; Bio-Rad Laboratories, Hercules, CA), and standard PCR reactions were performed. All primers were designed to anneal within exons, with each pair spanning at least one intron (primer sequences provided in Supplementary Table S1, http://www.iovs.org/lookup/suppl/doi:10.1167/iovs.10-5993/-/DCSupplemental). PCR products were analyzed on 2.5% agarose gels using EtBr detection.

Western Blot Analysis

Enucleated eyes were dissected into different parts as just described, and Western blots were performed as described elsewhere, with minor modifications.[18] Samples were homogenized with plastic pestles in lysis buffer (50 mM Tris-HCl [pH 7.4], 150 mM NaCl, 1 mM EDTA, 0.1% Triton X-100, and 0.1% SDS) supplemented with 1 mM PMSF and a mix of additional protease inhibitors (Halt Proteinase Inhibitor Cocktail; Thermo Scientific, Rockford, IL). Total tissue lysates were centrifuged, and protein concentration in the resulting supernatant was determined with the BCA protein assay reagent (Sigma-Aldrich, St Louis, MO). Fifty micrograms of lysate from each sample were electrophoresed on 7.5% SDS-PAGE gels and transferred to PVDF membranes (Millipore, Bedford, MA). The membranes were blocked at room temperature in 5% dry milk in TBST (Tris-buffered saline with 0.1% Tween-20) for 2 hours, followed by incubation with a rabbit anti-mouse SH3PXD2B polyclonal antibody[18] diluted at 1:1000 in TBS overnight at 4°C. The membranes were rinsed twice, washed four times for 5 minutes, each at room temperature in TBST with gentle shaking. They were then incubated in a 1:4000 dilution of horseradish peroxidase–conjugated goat anti-rabbit IgG (Invitrogen, Carlsbad, CA) for 30 minutes at room temperature and washed in TBST. Immunoreactivity was detected by enhanced chemiluminescence methodology (GE Health Care, Piscataway, NJ). Experiments were performed in triplicate on three independent samples of dissected tissues.

Results

Early-Onset Iridocorneal Adhesion in *nee* Mice

We have previously shown that by 1 month of age, B10-*Sh3pxd2b*^{nee} mice exhibit a form of anterior segment dysgenesis that is characterized by peripheral iridocorneal adhesions, enlarged anterior chambers, and corneal opacity.[18] To further examine the onset and progression of these phenotypes, we examined B10-*Sh3pxd2b*^{nee} mice with a slit lamp from early postnatal life through 10 months of age (Fig. 1). At P17, the eyes of littermate control mice had clear corneas, normal anterior chamber depth, and normal iridocorneal angles, with a sharply defined limbus (Figs. 1A–C, $n = 10$ eyes). Among the age-matched B10-*Sh3pxd2b*^{nee} mice, all eyes initially also exhibited clear corneas and normal anterior chamber depth (Figs. 1D, 1E), but unlike the eyes of the control mice, all eyes contained iridocorneal adhesions present throughout the entire circumference of the eye (Fig. 1F; Supplementary Fig. S1, http://www.iovs.org/lookup/suppl/doi:10.1167/iovs.10-5993/-/DCSupplemental; $n = 14$ eyes). At P17, the only additional ocular defect noted in B10-*Sh3pxd2b*^{nee} mice was occasionally misshapen pupils ($n = 3$ / 14 eyes). Whereas eyes of littermate controls remained unaffected throughout 10 months of age, the iridocorneal defects of B10-*Sh3pxd2b*^{nee} mice persisted and were followed by a course involving enlarged anterior chamber depth and corneal opacity (Figs. 1G–R, $n = 14$ eyes per genotype at 3 months of age and 6 eyes per genotype at 10 months of age). Enlargement of the anterior chamber and the emergence of focal corneal opacity were first observed in 1-month-old B10-*Sh3pxd2b*^{nee} mice. By 3 months of age, enlarged anterior chambers and/or corneal opacities were observed in all B10-*Sh3pxd2b*^{nee} mice, with corneal neovascularization frequently present by 10 months of age. These findings indicate that mutation of *Sh3pxd2b* disrupts normal development of the iridocorneal angle and ultimately results in a severe ocular disease influencing multiple tissues.

In addition to the changes to the iridocorneal angle, three additional phenotypes influencing the anterior segment were detected in B10-*Sh3pxd2b*^{nee} mice: decreased central corneal thickness (CCT), the development of cataracts, and hypopyon. CCT was measured because many forms of anterior segment dysgenesis influence the extracellular matrix of the corneal

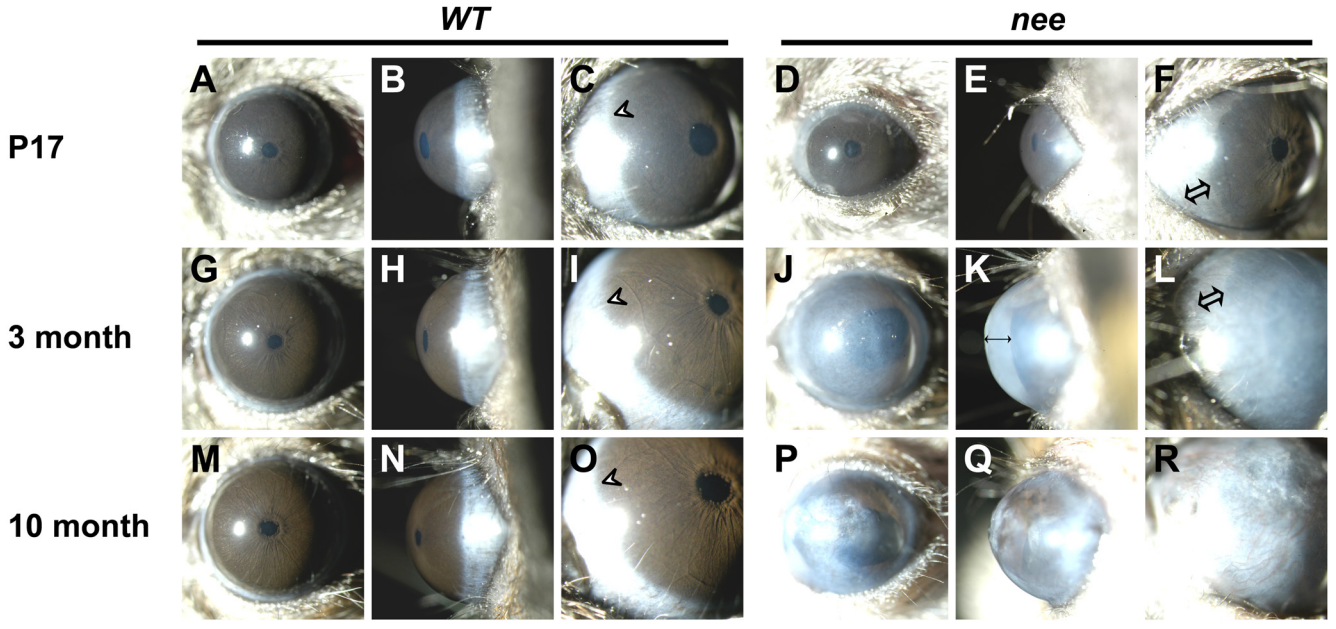

Figure 1. Slit lamp analysis of *nee* mice. Slit lamp images of eyes from littermate controls homozygous for the wild-type allele (WT) and B10-*Sh3pxd2b*^{nee} mice homozygous for the *Sh3pxd2b*^{nee} mutation (*nee*), showing early-onset iridocorneal adhesions and indices of glaucoma in *nee* mice. (**A–F**) At P17, both WT and *nee* mice had clear corneas and anterior chambers of normal depth. However, whereas WT mice had a sharply defined limbus (**C**, *arrowhead*), *nee* mice had iridocorneal adhesions (**F**, *double arrow*). An enlarged presentation of (**C**) and (**F**) with additional labels highlighting the synechia is available in Supplementary Figure S1 (http://www.iovs.org/lookup/suppl/doi:10.1167/iovs.10-5993/-/DCSupplemental). (**G–L**) At both 3 months of age and (**M–R**) 10 months of age, WT mice maintain normal-appearing eyes with a defined limbus (**I**, **O**, *arrowheads*), whereas the eyes of *nee* mice continued to exhibit iridocorneal adhesions (**L**, *double arrow*), as well as progressively enlarged anterior chambers (**K**, *double arrow*), corneal opacity, and corneal neovascularization.

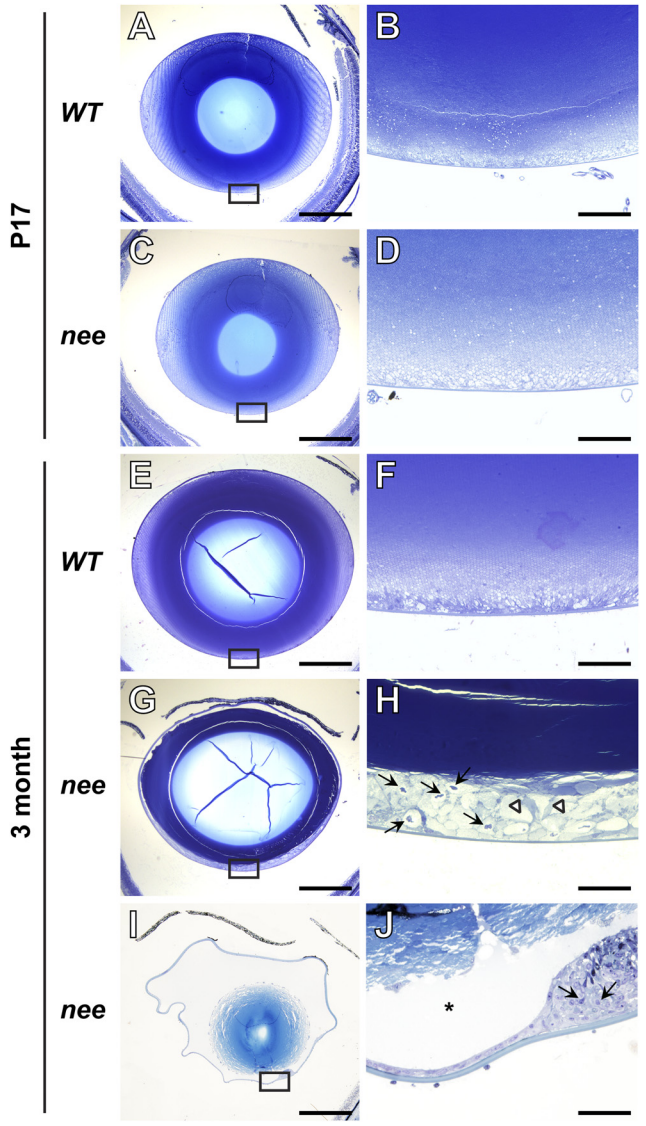

FIGURE 2. Lens phenotypes of *nee* mutants. Plastic sections stained with toluidine blue collected from littermate controls homozygous for the wild-type allele (WT) and B10-*Sh3pxd2b*^{nee} mice homozygous for the *Sh3pxd2b*^{nee} mutation (*nee*) showing the presence of cataract in *nee* mice. Boxed areas in low-magnification images are shown at higher magnification in the adjacent panels. (**A–D**) At P17, lenses of WT and *nee* mice were both normal in appearance. (**E**, **F**) At 3 months of age, lenses of WT mice remained normal. (**G**, **H**) Example of a lens from a 3-month-old *nee* mouse with posterior abnormalities, including posterior migration of epithelial cells (*arrows*). Posterior lens fibers also appeared enlarged (*arrowheads*). (**I**, **J**) Example of a lens from a 3-month-old *nee* mouse with hypermature cataract. Note cortex liquefaction (✱); a subcapsular cell plaque is also visible (*arrows*). Scale bar: (**A**, **C**, **E**, **G**, **I**) 500 μm; (**B**, **D**, **F**, **H**, **J**) 50 μm.

stroma, resulting in thin corneas. Measurements made with an ultrasound pachymeter revealed that B10-*Sh3pxd2b*^{nee} mice at 1 month of age exhibited a CCT of 60.49 ± 13.98 μm (mean ± SD; n = 7 eyes), whereas littermate controls had a CCT of 93.49 ± 3.53 μm (mean ± SD; n = 8 eyes; P = 0.0006, Student's two-tailed t-test). Thus, the *Sh3pxd2b*^{nee} mutation causes a developmental defect of the cornea. Because the cornea becomes opaque at later stages, CCT was not measured in older mice. In the case of cataract formation (Fig. 2), we noted that the lenses appeared normal at P17, but that abnormalities frequently appeared by 3 months of age. Histologic examination at P17 revealed normal lens morphology (Figs. 2A–D). By 3 months of age, however, the lenses in approximately 50% of the eyes exhibited defects. Among the lenses with mild lens phenotypes, defects occurred posteriorly where migrated cells, typically appearing swollen, were often present (n = 4/19 eyes at 3 months), indicating a posterior subcapsular cataract (Figs. 2E–H). Among the lenses with more severe defects (Figs. 2I, 2J and Supplementary Fig. S2, http://www.iovs.org/lookup/suppl/doi:10.1167/iovs.10-5993/-/DCSupplemental), many contained hypermature cataracts characterized by complete cortical and nuclear opacification with a wrinkled lens capsule (n = 7/19 eyes at 3 months). Gradual worsening was observed in mice that were 9 to 15 months of age; by this time, all eyes exhibited some form of lens abnormality ranging from the presence of posteriorly located swollen cells (n = 5/8 eyes) to hypermature cataracts (n = 3/8). Because of corneal opacity, it was generally not possible to document the occurrence of cataracts with slit lamp examination, although some severe instances and hypermature cataracts were occasionally visible (Supplementary Fig. S3, http://www.iovs.org/lookup/suppl/doi:10.1167/iovs.10-5993/-/DCSupplemental). In the case of hypopyon (Fig. 3), histologic analysis of eyes from B10-*Sh3pxd2b*^{nee} mice not only demonstrated the uniform presence of iridocorneal adhesions (Figs. 3A, 3B), but also the occasional presence of large, inferiorly located pools of white cellular infiltrate (Fig. 3C). Hypopyon was also evident by slit lamp examination in B10-*Sh3pxd2b*^{nee} mice at 3 months of age (Fig. 3D; n = 6/16 eyes), but not in any of their wild-type littermates. Hypopyon was not observed in any eyes at P17. Therefore, inflammation cannot explain the severe iridocorneal adhesions in B10-*Sh3pxd2b*^{nee} mice, but rather they seem to be an additional consequence of the severe ocular disease that occurs in the mice. In contrast to the anterior segment,

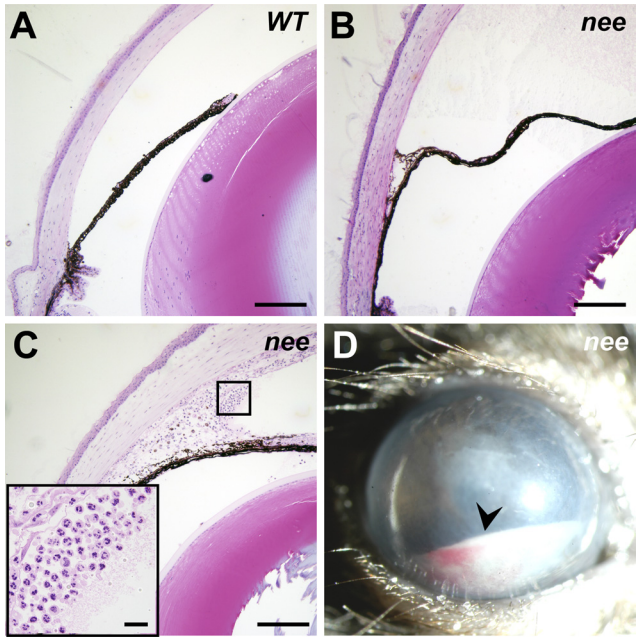

FIGURE 3. Anterior chamber phenotypes in *nee* mice. Plastic sections stained with H&E from littermate controls homozygous for the wild-type allele (WT) and B10-*Sh3pxd2b*^{nee} mice homozygous for the *Sh3pxd2b*^{nee} mutation (*nee*). (**A**) Normal iridocorneal angle morphology in WT mice versus (**B**) iridocorneal adhesion in *nee* mice and (**C**) hypopyon in *nee* mice. Note from the boxed area shown at higher magnification that the infiltrate was cellular. Images from mice 4 to 5 months in age. (**D**) Slit lamp image from a 3-month-old *nee* mouse showing hypopyon (*arrowhead*). Mild hyphema was also present. Scale bar: (**C**) 200 μm; (*inset*) 20 μm.

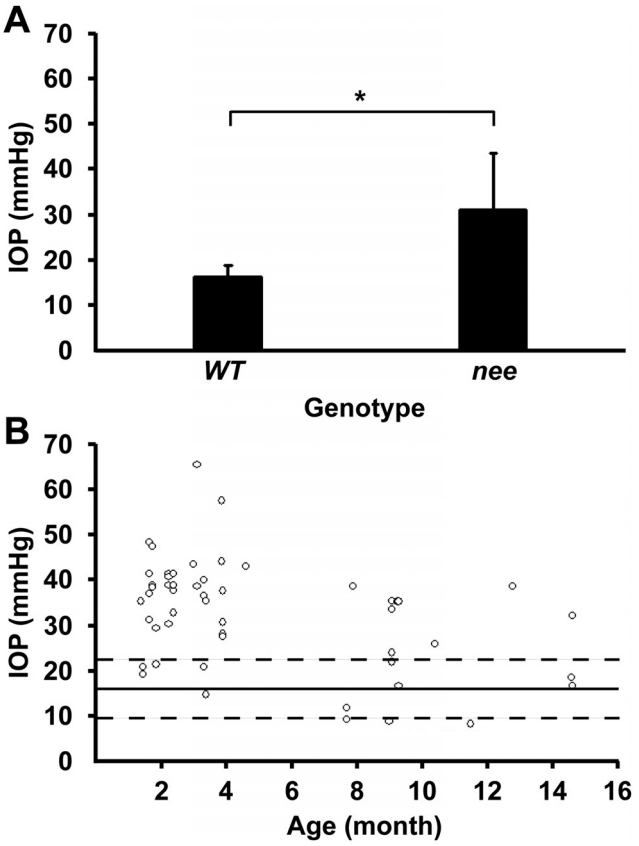

Figure 4. IOP profile of *nee* mice. IOP measured with a microneedle cannulation system, showing that IOP was elevated in *nee* mice. (**A**) Comparison of IOP from cohorts of littermate controls homozygous for the wild-type allele (WT) and B10-*Sh3pxd2b*^{nee} mice homozygous for the *Sh3pxd2b*^{nee} mutation (*nee*) at 3 to 4 months of age. Mean ± SD; $^{*}P = 0.0006$, Student's two-tailed *t*-test. (**B**) IOP values from individual *nee* mice of various ages. The mean IOP of WT mice at 3 to 4 months of age (*solid line*) ± 2.5 SD (*dashed lines*) are shown.

posterior segment infiltration was uncommon, with only 2 of 19 eyes of B10-*Sh3pxd2b*^{nee} mice having detectable leukocytes, in both cases from eyes also containing hypermature cataracts.

Elevated Intraocular Pressure in *nee* Mice

To directly test whether the eyes of B10-*Sh3pxd2b*^{nee} mice with iridocorneal adhesions exhibit IOP elevation, IOP was measured in cohorts of B10-*Sh3pxd2b*^{nee} and littermate control mice (Fig. 4). In B10-*Sh3pxd2b*^{nee} mice, a significant elevation of IOP was readily apparent at 3 to 4 months of age (Fig. 4A). Whereas littermate control mice exhibited an IOP of 16.0 ± 2.6 mm Hg (mean ± SD; $n = 15$ eyes), a value within the range of pressures normally observed among several nonglaucomatous strains of inbred mice,[24] B10-*Sh3pxd2b*^{nee} mice had a significantly elevated IOP of 30.8 ± 12.5 mm Hg (mean ± SD; $n = 15$ eyes; $P = 0.0006$, Student's two-tailed *t*-test). Similar elevated IOP values in B10-*Sh3pxd2b*^{nee} mice were observed at all ages tested, with significantly elevated IOP observed at the earliest and latest time points tested (1.4–14.6 months of age; Fig. 4B). These data indicate that the *Sh3pxd2b*^{nee} mutation causes a significant elevation of IOP which can remain elevated for substantial periods of time and is likely to cause glaucomatous damage.

Retinal Ganglion Cell Loss and Optic Nerve Head Excavation in *nee* Mice

To further determine the consequences of *Sh3pxd2b* mutation on the eye, we examined the retinas of B10-*Sh3pxd2b*^{nee} mice histologically (Fig. 5). At P17, the retinas of B10-*Sh3pxd2b*^{nee} and littermate control mice were indistinguishable ($n = 11$ eyes per genotype), with both appearing morphologically normal (Figs. 5A, 5B). At 3 months of age, the retinas of littermate control mice remained normal in appearance ($n = 12$ eyes), whereas all retinas of B10-*Sh3pxd2b*^{nee} mice showed indices of glaucomatous damage ($n = 19$ eyes), including thinning of the

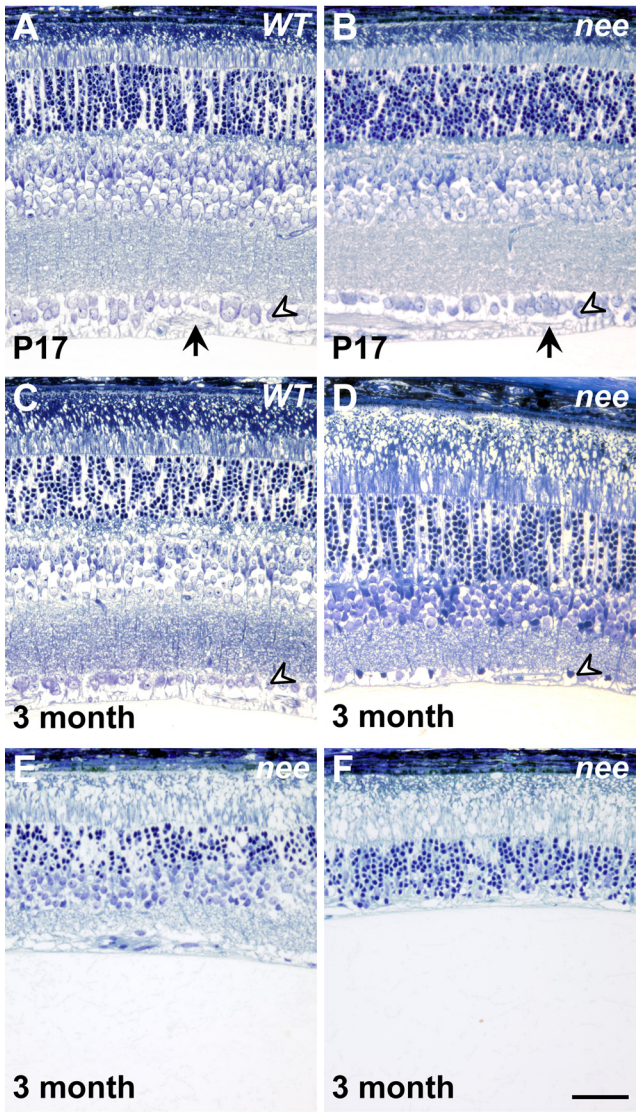

Figure 5. Retinal phenotypes of *nee* mice. Position-matched images from plastic sections stained with toluidine blue. Comparison of littermate controls homozygous for the wild-type allele (WT) and B10-*Sh3pxd2b*^{nee} mice homozygous for the *Sh3pxd2b*^{nee} mutation (*nee*) revealed glaucomatous changes in the retinas of *nee* mice. (**A**, **B**) At P17, the retinas of WT and *nee* mice were indistinguishable, with all laminae present, a robust nerve fiber layer (*arrows*), and continuous ganglion cell layer that was one to two cells thick (*arrowheads*). (**C–F**) At 3 months of age, WT mice maintained a normal-appearing retina, whereas *nee* mice had lost cells from the retinal ganglion cell layer (**C**, *arrowhead*) and the nerve fiber layer had thinned. Variable degrees of panretinal thinning were observed, ranging from mild (as observed in **D**) to progressively severe (as observed in **E**, **F**). Scale bar, 200 μm.

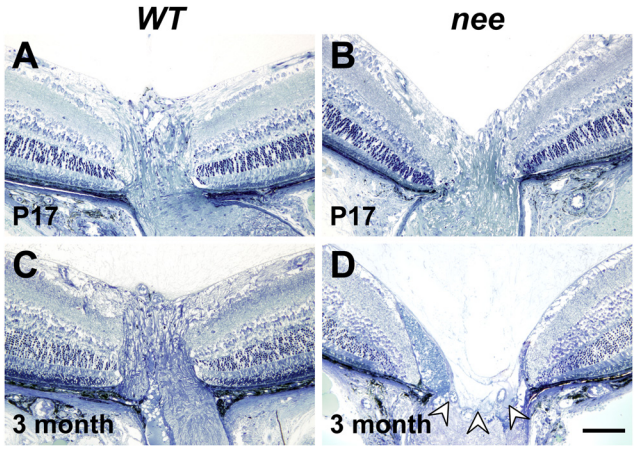

FIGURE 6. Optic nerve head phenotypes of *nee* mice. Plastic sections stained with toluidine blue from littermate controls homozygous for the wild-type allele (WT, *left column*) and B10-*Sh3pxd2b*^{nee} mice homozygous for the *Sh3pxd2b*^{nee} mutation (*nee, right column*), revealing optic nerve head excavation in *nee* mice. (**A**, **B**) At P17, the optic nerve head of WT and *nee* homozygotes was normal, with a thick nerve fiber layer. (**C**, **D**) At 3 months of age, WT mice maintained a normal-appearing optic nerve head, whereas *nee* mice exhibited severe excavation (*arrowheads*) that extended beyond the choroid. Scale bar, 150 μm.

nerve fiber layer and a striking loss of retinal ganglion cells (Figs. 5C–F). Similar to what has been observed in other mouse models of glaucoma,[24,25] panretinal thinning involving multiple layers was observed to various degrees in B10-*Sh3pxd2b*^{nee} eyes with increasing age (Figs. 5D–F). Loss of ganglion cells was accompanied by severe optic nerve head excavation (Fig. 6). At P17, the optic nerve head appeared normal in both B10-*Sh3pxd2b*^{nee} and littermate control mice (n = 11 eyes per genotype) and was characterized by a robust nerve fiber layer (Figs. 6A, 6B). While the optic nerve head of littermate controls changed little with age, all B10-*Sh3pxd2b*^{nee} eyes had advanced optic nerve head atrophy by 3 months of age (n = 11 eyes per genotype; Figs. 6C, 6D). Combined, these findings indicate that the *Sh3pxd2B* mutation has little or no influence on overall development of the retina, which appeared normal at P17, but that soon thereafter it causes severe glaucomatous damage to retinal ganglion cells and ultimately to all layers of the retina.

Optic Nerve Damage in *nee* Mice

To quantify the glaucomatous damage, cross sections of the optic nerve from B10-*Sh3pxd2b*^{nee} mice stained with PPD were analyzed histologically (Fig. 7). At P17, axons within the optic nerves of both littermate control and B10-*Sh3pxd2b*^{nee} mice appeared healthy, containing tightly packed myelin sheaths surrounding individual axons (Figs. 7A, 7B). The total number of myelinated axons at P17 differed slightly between genotypes, with littermate control mice having 25,860 ± 3,656 axons (mean ± SD; n = 13) and B10-*Sh3pxd2b*^{nee} mice having 20,988 ± 2,183 axons (mean ± SD; n = 10; P = 0.0008, Student's two-tailed t-test). As has been observed in other instances,[26–28] there was a correlation between dimensions of the optic nerve and body size. The change in axon numbers observed at P17 corresponds to the overall reduction in body mass of B10-*Sh3pxd2b*^{nee} mice,[18] which at P17 are approximately 15% smaller than littermate control mice (mass of B10-*Sh3pxd2b*^{nee} females = 6.6 ± 0.3 g, mean ± SD, n = 6; mass of littermate control females = 7.8 ± 1.2 g, mean ± SD, n = 9; P = 0.026, Student's two-tailed t-test). While the optic nerve axons of littermate control mice completed myelination and remained healthy in appearance with increasing age, those of B10-*Sh3pxd2b*^{nee} mice underwent degeneration, as evident from both qualitative (Figs. 7C, 7D) and quantitative (Fig. 7E) analyses. By 3 months of age, nearly all axons within the optic nerves of B10-*Sh3pxd2b*^{nee} mice had degenerated, and the remaining tissue was gliotic. The total number of myelinated axons in littermate control mice was 48,223 ± 7,147 (mean ± SD; n = 8; range, 38,130–57,369), and that in B10-*Sh3pxd2b*^{nee} mice was 550 ± 686 (mean ± SD; n = 16;

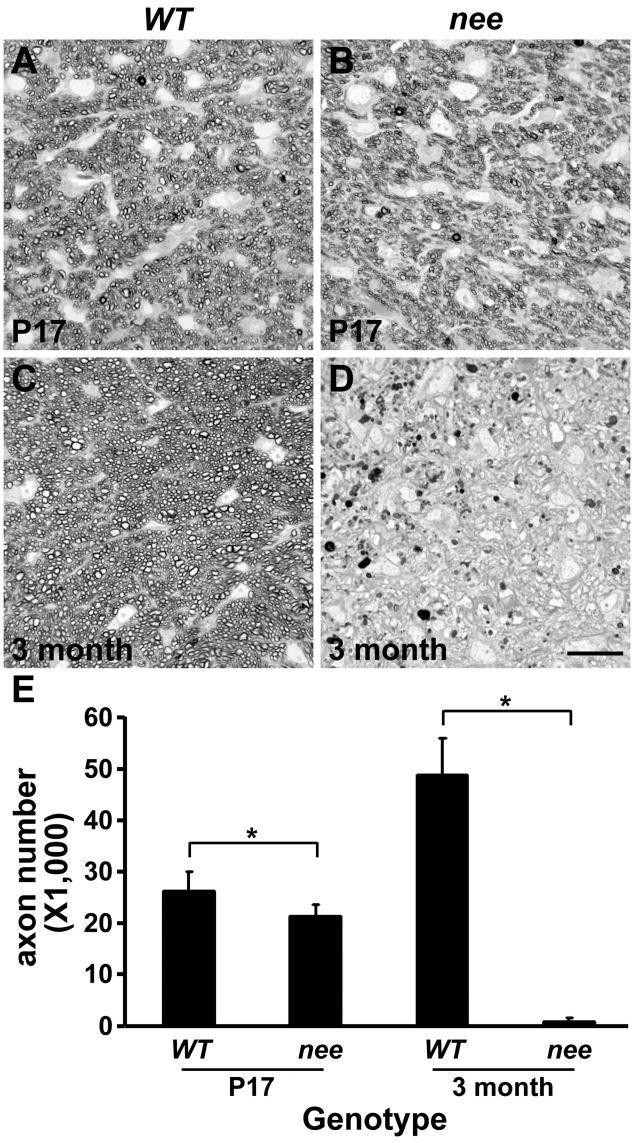

FIGURE 7. Optic nerve phenotypes of *nee* mice. Optic nerve cross sections from littermate controls homozygous for the wild-type allele (WT) and B10-*Sh3pxd2b*^{nee} mice homozygous for the *Sh3pxd2b*^{nee} mutation (*nee*) stained with PPD, which stains the myelin sheath of healthy optic nerves and the axoplasm of damaged axons, showing axon degeneration of *nee* mice. (**A**, **B**) At P17, optic nerves of WT and *nee* mice contained healthy appearing axons. In *nee* mice, axons appeared to be sparser than in WT mice, yet no signs of damaged axons were visible. Because myelination was not yet complete at this stage, PPD-stained axons were sparser than in adult optic nerves. (**C, D**) At 3 months of age, optic nerves of WT mice were densely packed with healthy-appearing myelinated axons, whereas optic nerves from *nee* mice were characterized by severe axon degeneration and areas of gliosis. Scale bar, 20 μm. (**E**) Quantification of the axons (mean ± SD; n = 8–16 optic nerves quantified per genotype). *$P < 0.001$.

range, 16–2,660; $P = 2.7 \times 10^{-7}$, Student's two-tailed *t*-test). The optic nerve phenotype of B10-*Sh3pxd2b*^{nee} mice exhibited complete penetrance, with no nerves escaping severe damage. These results uncover a subtle developmental abnormality within the optic nerve of B10-*Sh3pxd2b*^{nee} mice and confirm the presence of an aggressive form of early-onset glaucoma.

The glaucomatous progression of B10-*Sh3pxd2b*^{nee} mice was also evident from analysis of the cross-sectional area of the optic nerve. In mice, retinal ganglion cells are generated from embryonic day (E)11 to just before birth and from postnatal day (P)0 to P12 undergo a wave of developmental cell death that removes approximately two of three of the cells.[29–32] Myelination of retinal ganglion cell axons begins around P5, is intense during weeks 2 to 5 and complete by week 16.[33] As a consequence of these events, the cross-sectional area of the optic nerve grows rapidly during the first 5 weeks of postnatal life and thereafter remains relatively stable.[34] Conversely, as retinal ganglion cells die in glaucoma, the cross-sectional area of the optic nerve typically decreases.[20,35] At P17, the cross-sectional area of the optic nerve in B10-*Sh3pxd2b*^{nee} mice (63,868 ± 8,225 μm^2, mean ± SD; $n = 13$) was slightly less than that in the littermate control mice (65,029 ± 8,453 μm^2, mean ± SD; $n = 10$), but the difference was not statistically significant. At 3 months of age, the cross-sectional area of the optic nerve in B10-*Sh3pxd2b*^{nee} mice (40,807 ± 13,187 μm^2, mean ± SD; $n = 16$), was significantly reduced in comparison to that in the age-matched littermate control mice (82,545 ± 16,705 μm^2, mean ± SD; $n = 9$, $P = 1.7 \times 10^{-5}$, Student's two-tailed *t*-test) again indicating that B10-*Sh3pxd2b*^{nee} mice undergo a severe glaucomatous progression.

Ocular Distribution of *Sh3pxd2b*

To identify ocular tissues in which *Sh3pxd2b* may be most important in contributing to anterior segment dysgenesis and early-onset glaucoma, ocular distribution of *Sh3pxd2b* was tested in pools of dissected mouse tissues by RT-PCR (Fig. 8A) and Western blot (Supplementary Fig. S4, http://www.iovs.org/lookup/suppl/doi:10.1167/iovs.10-5993/-/DCSupplemental). Consistent with several published microarray studies suggesting a broad ocular expression,[19,36–41] *Sh3pxd2b* transcript was detected in all ocular tissues tested. Similar results were obtained with Western blot analysis, with the exception that SH3PXD2B protein was not detected in the lens, whereas *Sh3pxd2b* transcripts were. Because the only known molecular function of *Sh3pxd2b* pertains to podosomes,[15] expression of several podosome-related genes were also tested for potential co-expression with *Sh3pxd2b* in pools of dissected mouse tissues by RT-PCR (Fig. 8B). Among candidates involved in the assembly of the podosomes (*Cttn*, *Src*, and *Wasl*)[42–44] or extracellular matrix regulation (*Adam15*, *Adam19*, and *Mmp14*),[15,18,45–46] all were expressed in the same broad distribution as *Sh3pxd2b* (the only exception being that the *Adam15*, *Adam19*, and *Mmp14* transcripts were not detectable in the lens). While not informative with regard to focusing attention on a given tissue, these data demonstrate that *Sh3pxd2b* and other genes important to podosomes are widely expressed in multiple ocular tissues, perhaps indicating that podosomes could play multiple roles throughout the eye.

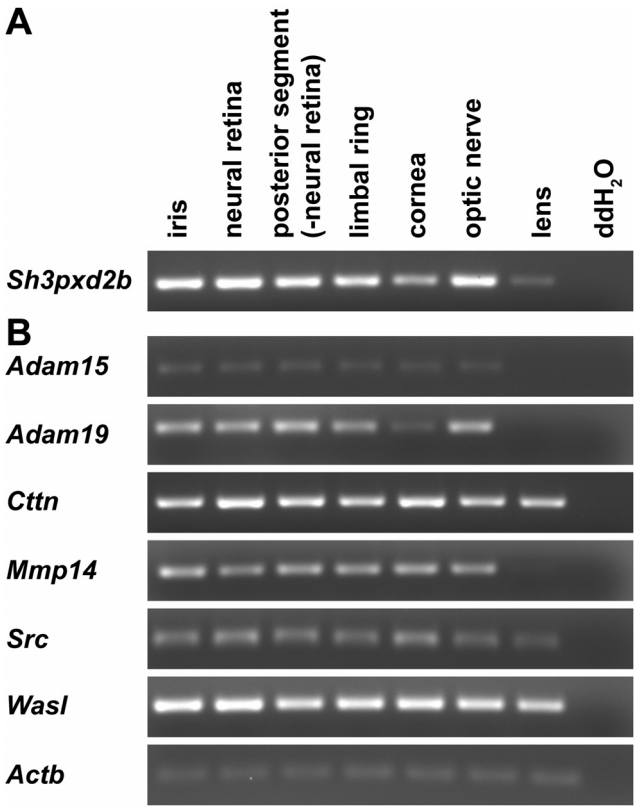

FIGURE 8. Ocular distribution of *Sh3pxd2b* and podosome-related genes. PCR products of RT-PCR reactions with pools of dissected mouse tissues analyzed on 2.5% agarose gels using EtBr detection. (**A**) *Sh3pxd2b* and (**B**) candidates involved in the assembly of podosomes or extracellular matrix regulation were widely expressed in the eye.

DISCUSSION

In humans, mutations in *SH3PXD2B* cause Frank-Ter Haar syndrome, a rare condition involving congenital glaucoma. Here, we have provided evidence that B10-*Sh3pxd2b*^{nee} mice exhibit anterior segment dysgenesis that causes a form of early-onset glaucoma. The etiology we observed primarily involves severe iridocorneal adhesions which presumably block aqueous humor outflow and cause drastic IOP elevation, after which retinal degeneration and optic nerve cupping ensue. SH3PXD2B is predicted to be a podosome adaptor protein that limits the membrane localization of metalloproteinases to specific domains for coordinated interaction with the extracellular matrix. Thus, these data identify B10-*Sh3pxd2b*^{nee} mice as a new mouse model of glaucoma, implicate podosomes in normal development of the iridocorneal angle, and suggest that additional genes that influence podosomes are candidates worthy of consideration as contributors to developmental forms of glaucoma.

Mechanisms Underlying *Sh3pxd2b*-Mediated Defects

Although much is known about the embryonic origin of anterior segment structures, little is known about the molecular events that are required for their normal development. The mammalian eye is derived from three major tissue types: surface ectoderm, neuronal ectoderm, and periocular mesenchyme (a loose array of cells of neural crest and mesodermal origin). Most iridocorneal angle structures are derived from the periocular mesenchyme, including the corneal stroma, corneal endothelium, ciliary stroma and smooth muscles, iris stroma, and trabecular meshwork.[47,48] In mice, neural crest–derived cells first migrate into the presumptive anterior chamber at E10.5, and by E14.5 they represent the major cell type of the presumptive iridocorneal angle, although mesodermal cells are also present.[49] At E12.5 to E14.5, the periocular mesenchyme migrates to establish the presumptive corneal stroma, which

becomes the major determinant of corneal thickness.[19] A separation between the iris and cornea, the first appearance of an iridocorneal angle recess, is typically first evident at E16.5.[50] Development and remodeling of the iridocorneal angle, especially of the drainage structures, continues well into postnatal development, with intratrabecular spaces opening to allow a gradual outflow of the aqueous humor from P14 to P42.[47,50] In B10-*Sh3pxd2b*^{nee} mice, the iris and cornea appear never to separate. From histologic analyses performed to date, we have also been unable to definitively detect the periocular mesenchymal-derived Schlemm's canal or trabecular meshwork in B10-*Sh3pxd2b*^{nee} mice (data not shown). Whereas some periocular mesenchyme-derived structures of B10-*Sh3pxd2b*^{nee} mice were disrupted, others such as the corneal endothelium and iris stroma appeared normal. Thus, much of the migration of mesenchymal cells into the anterior segment structures and their differentiation occurs normally. Combined, the presence of iridocorneal adhesions and decreased corneal thickness in B10-*Sh3pxd2b*^{nee} mice likely indicates a focal deficiency resulting from altered migration or differentiation of a subset of periocular mesenchymal cells. Although the experiments described here do not directly examine these early stages of development, they do identify *Sh3pxd2b* as a gene important to anterior segment development and suggest that mice with the *Sh3pxd2b*^{nee} mutation will be a useful resource for future studies of these stages in ocular development.

Among genes known to be associated with anterior segment dysgenesis in mice or humans,[47,48] several are thought to influence the extracellular matrix. For example, mutations disrupting *Foxc1*, *Bmp4*, *Col4a1*, and *Gpr48* all cause forms of anterior segment dysgenesis involving iridocorneal adhesion, and all these genes are also known to influence various aspects of extracellular matrix.[26,51–54] Likewise, several additional genes associated with anterior segment dysgenesis also share links to the extracellular matrix, including genes influencing collagens,[26,55] ADAMs,[56] and members of the TGFβ superfamily.[51,57] The extracellular matrix has a well-established role in regulating the function of the mature trabecular meshwork.[58] However, it is less clear how the extracellular matrix influences development of the trabecular meshwork or iridocorneal angle, very likely influencing both cellular migration and differentiation events.[59–61]

The structure of the SH3PXD2B protein also provides hints about the mechanisms that most likely contribute to the pathology in B10-*Sh3pxd2b*^{nee} mice. SH3PXD2B belongs to the SH3 and PX domain-containing family of proteins.[14,15] Currently, this family includes two members, SH3PXD2A and SH3PXD2B; both are predicted by published microarray expression studies to be broadly expressed throughout the eye.[19,36–41] Through their SH3 domains, these proteins can interact with or recruit a variety of other proteins encoded by genes that we have shown are widely distributed with *Sh3pxd2b* throughout the eye, including the actin nucleation factor WASL; the adaptor protein CTTN; and transmembrane metalloproteinases such as ADAM15, ADAM19, and MMP14.[15,18,45,62,63] The PX domains of SH3PXD2A and SH3PXD2B are known to interact with multiple phosphoinositides, including PtdIns(3,4)P_2.[14,15,45]Most of these molecules are involved in the assembly or function of podosomes. Therefore, SH3PXD2A and SH3PXD2B have been implicated in podosome-related activities such as extracellular matrix modulation, cell migration, and invasion. Although podosomes have not been observed in ocular tissue during development, they have been observed in cells derived from adult ocular tissues, notably in cells of the trabecular meshwork.[17] Although speculative, these findings suggest that SH3PXD2B may regulate localization of a metalloproteinase involved in migration and/or function of mesenchymal-derived trabecular meshwork cells responsible for regulating the density of the trabecular meshwork extracellular matrix. Alternatively, SH3PXD2A and SH3PXD2B might interact with a metalloproteinase with sheddase activity, a mechanism that would be equally capable of contributing to anterior segment dysgenesis.[56] Metalloproteinases have been suggested to contribute to several disease processes of the anterior segment, including glaucoma and cataractogenesis.[64,65] In sum, the current findings suggest that the *Sh3pxd2b*^{nee} mutation contributes to a form of anterior segment dysgenesis involving glaucoma and cataracts through misregulation of metalloproteinases.

Mouse Models of Glaucoma

Mouse models are useful tools for studying the basic biology of glaucoma, identifying glaucoma-causing genes and testing the efficacy of potential medical treatments. Among the small number of mouse strains described to have forms of glaucoma,[24,66–71] the most widely used currently is the DBA/2J model.[72,73] As a consequence of a pigment dispersing iris disease, DBA/2J mice begin to exhibit elevated IOP after 6 months of age and most optic nerves are severely damaged by 12 months of age.[72] A significant advantage of B10-*Sh3pxd2b*^{nee} mice as a model of glaucoma is the occurrence of glaucoma without the necessity for extensive aging. Thus, the model allows faster experimental timeframes and reduced animal housing costs. Furthermore, the aggressive nature of the glaucoma in B10-*Sh3pxd2b*^{nee} mice may allow smaller animal cohorts than required for use with DBA/2J mice, where penetrance and asymmetry of disease progression are experimental challenges that are typically overcome by use of large animal cohorts.[72,73]

Although likely to be useful in many settings, use of B10-*Sh3pxd2b*^{nee} mice as a model of glaucoma also has several caveats that must be considered in designing experiments and interpreting data. First, the elevation of IOP in B10-*Sh3pxd2b*^{nee} mice is profound, and it is likely that the consequences of a dramatic elevation in IOP in young eyes will not fully reflect those that arise in all forms of glaucoma, many of which are associated with a modest but persistent elevation in IOP in older eyes. Second, the presence of corneal opacity and cataracts in B10-*Sh3pxd2b*^{nee} mice obstruct the ability to view the fundus and optic nerve head, degrading the ability to perform experiments based on in vivo imaging. Likewise, corneal disease also makes it impractical to use noninvasive instruments such as rebound tonometers to measure IOP, making it more difficult to estimate IOP exposure over time. Third, studies of the glaucomatous neurodegeneration that occurs in B10-*Sh3pxd2b*^{nee} mice may be complicated by the rapid damage also occurring in other retinal layers. Although retinal thinning is typically not a feature of human glaucoma, it has been observed in other glaucomatous mouse strains.[24,25] Finally, it is still unclear which phenotypes of B10-*Sh3pxd2b*^{nee} mice are cell autonomous and which are secondary consequences of the severe eye disease the mice undergo. A key question regarding this pertains to the ocular expression of *Sh3pxd2b*. Our current work demonstrates a very broad tissue distribution, but it is important to also examine expression at the cellular level. Unfortunately, we have thus far been unable to find conditions allowing our SH3PXD2B antibody to work specifically in immunohistochemistry of ocular sections. Distribution of *Sh3pxd2b* studied with in situ hybridization has been partially presented elsewhere[13]; completing a characterization of transcript and protein localization is of clear importance in further mechanistic studies.

In conclusion, this study demonstrates that eyes of B10-*Sh3pxd2b*^{nee} mice exhibit multiple features of congenital glaucoma. These findings implicate podosomes in the nor-

mal development of the iridocorneal angle and establish the B10-*Sh3pxd2b*^{nee} strain as a new mouse model of glaucoma with potentially significant benefits over those that have been studied to date. Because the *nee* mutation arose on an infrequently used genetic background (B10.A-*H2*^{b4}/(4R)SgDvEg), we have generated an N10 congenic strain of mice transferring the *Sh3pxd2b*^{nee} mutation to the widely used C57BL/6J genetic background. In our ongoing work, we intend to complete a comparative analysis of disease features in this congenic strain and to use it to continue a genetic analysis of podosome-related contributions to anterior-segment dysgenesis and glaucoma.

Acknowledgments

The authors thank Rob Mullins, John Fingert, Bo Chang, and Norm Hawes for many helpful discussions; Sachiyo Iwashita for help in maintaining the mouse colonies; Geoffrey Lively for his contribution to measuring corneal thickness; and Olga Savinova for technical assistance with IOP recordings.

References

1. Kwon YH, Fingert JH, Kuehn MH, Alward WL. Primary open-angle glaucoma. *N Engl J Med.* 2009;360:1113–1124.
2. Quigley HA, Broman AT. The number of people with glaucoma worldwide in 2010 and 2020. *Br J Ophthalmol.* 2006;90:262–267.
3. Kass MA, Heuer DK, Higginbotham EJ, et al. The Ocular Hypertension Treatment Study: a randomized trial determines that topical ocular hypotensive medication delays or prevents the onset of primary open-angle glaucoma. *Arch Ophthalmol.* 2002;120:701–713; discussion 829–730.
4. McKinnon SJ, Goldberg LD, Peeples P, Walt JG, Bramley TJ. Current management of glaucoma and the need for complete therapy. *Am J Manag Care.* 2008;14:S20–S27.
5. Allingham RR, Liu Y, Rhee DJ. The genetics of primary open-angle glaucoma: a review. *Exp Eye Res.* 2009;88:837–844.
6. Wiggs JL. Genetic etiologies of glaucoma. *Arch Ophthalmol.* 2007; 125:30–37.
7. Tumer Z, Bach-Holm D. Axenfeld-Rieger syndrome and spectrum of PITX2 and FOXC1 mutations. *Eur J Hum Genet.* 2009;17:1527–1539.
8. Dai JX, Johnson RL, Ding YQ. Manifold functions of the Nail-Patella Syndrome gene Lmx1b in vertebrate development. *Dev Growth Differ.* 2009;51:241–250.
9. Morales J, Al-Sharif L, Khalil DS, et al. Homozygous mutations in ADAMTS10 and ADAMTS17 cause lenticular myopia, ectopia lentis, glaucoma, spherophakia, and short stature. *Am J Hum Genet.* 2009;85:558–568.
10. Azzedine H, Bolino A, Taieb T, et al. Mutations in MTMR13, a new pseudophosphatase homologue of MTMR2 and Sbf1, in two families with an autosomal recessive demyelinating form of Charcot-Marie-Tooth disease associated with early-onset glaucoma. *Am J Hum Genet.* 2003;72:1141–1153.
11. Dundar M, Saatci C, Tasdemir S, Akcakus M, Caglayan AO, Ozkul Y. Frank-ter Haar syndrome with unusual clinical features. *Eur J Med Genet.* 2009;52:247–249.
12. Frank Y, Ziprkowski M, Romano A, et al. Megalocornea associated with multiple skeletal anomalies: a new genetic syndrome? *J Genet Hum.* 1973;21:67–72.
13. Iqbal Z, Cejudo-Martin P, de Brouwer A, et al. Disruption of the podosome adaptor protein TKS4 (SH3PXD2B) causes the skeletal dysplasia, eye, and cardiac abnormalities of Frank-Ter Haar Syndrome. *Am J Hum Genet.* 2010;86:254–261.
14. Hishida T, Eguchi T, Osada S, Nishizuka M, Imagawa M. A novel gene, fad49, plays a crucial role in the immediate early stage of adipocyte differentiation via involvement in mitotic clonal expansion. *FEBS J.* 2008;275:5576–5588.
15. Buschman MD, Bromann PA, Cejudo-Martin P, Wen F, Pass I, Courtneidge SA. The novel adaptor protein Tks4 (SH3PXD2B) is required for functional podosome formation. *Mol Biol Cell.* 2009; 20:1302–1311.
16. Gimona M, Buccione R, Courtneidge SA, Linder S. Assembly and biological role of podosomes and invadopodia. *Curr Opin Cell Biol.* 2008;20:235–241.
17. Aga M, Bradley JM, Keller KE, Kelley MJ, Acott TS. Specialized podosome- or invadopodia-like structures (PILS) for focal trabecular meshwork extracellular matrix turnover. *Invest Ophthalmol Vis Sci.* 2008;49:5353–5365.
18. Mao M, Thedens DR, Chang B, et al. The podosomal-adaptor protein SH3PXD2B is essential for normal postnatal development. *Mamm Genome.* 2009;20:462–475.
19. Lively GD, Jiang B, Hedberg-Buenz A, et al. Genetic dependence of central corneal thickness among inbred strains of mice. *Invest Ophthalmol Vis Sci.* 2010;51:160–171.
20. John SW, Hagaman JR, MacTaggart TE, Peng L, Smithes O. Intraocular pressure in inbred mouse strains. *Invest Ophthalmol Vis Sci.* 1997;38:249–253.
21. Smith RS, Zabaleta A, John SW, et al. General and special histopathology. In: Smith RS, ed. *Systemic Evaluation of the Mouse Eye*. Boca Raton, FL: CRC Press; 2002:265–297.
22. Anderson MG, Libby RT, Mao M, et al. Genetic context determines susceptibility to intraocular pressure elevation in a mouse pigmentary glaucoma. *BMC Biol.* 2006;4:20.
23. Trantow CM, Hedberg-Buenz A, Iwashita S, Moore SA, Anderson MG. Elevated oxidative membrane damage associated with genetic modifiers of Lyst-mutant phenotypes. *PLoS Genet.* 2010;6: e1001008.
24. Anderson MG, Smith RS, Savinova OV, et al. Genetic modification of glaucoma associated phenotypes between AKXD-28/Ty and DBA/2J mice. *BMC Genet.* 2001;2:1.
25. Bayer AU, Neuhardt T, May AC, et al. Retinal morphology and ERG response in the DBA/2NNia mouse model of angle-closure glaucoma. *Invest Ophthalmol Vis Sci.* 2001;42:1258–1265.
26. Gould DB, Marchant JK, Savinova OV, Smith RS, John SW. Col4a1 mutation causes endoplasmic reticulum stress and genetically modifiable ocular dysgenesis. *Hum Mol Genet.* 2007;16:798–807.
27. Gould DB, Phalan FC, Breedveld GJ, et al. Mutations in Col4a1 cause perinatal cerebral hemorrhage and porencephaly. *Science.* 2005;308:1167–1171.
28. Noguchi T, Sugisaki T, Kudo M, Satoh I. Retarded growth of the suprachiasmatic nucleus and pineal body in dw and lit dwarf mice. *Brain Res.* 1986;391:161–172.
29. Drager UC. Birth dates of retinal ganglion cells giving rise to the crossed and uncrossed optic projections in the mouse. *Proc R Soc Lond B Biol Sci.* 1985;224:57–77.
30. Linden R, Pinto LH. Developmental genetics of the retina: evidence that the pearl mutation in the mouse affects the time course of natural cell death in the ganglion cell layer. *Exp Brain Res.* 1985;60:79–86.
31. Strom RC, Williams RW. Cell production and cell death in the generation of variation in neuron number. *J Neurosci.* 1998;18: 9948–9953.
32. Young RW. Cell death during differentiation of the retina in the mouse. *J Comp Neurol.* 1984;229:362–373.
33. Dangata YY, Kaufman MH. Myelinogenesis in the optic nerve of (C57BL x CBA) F1 hybrid mice: a morphometric analysis. *Eur J Morphol.* 1997;35:3–17.
34. Dangata YY, Findlater GS, Kaufman MH. Postnatal development of the optic nerve in (C57BL x CBA)F1 hybrid mice: general changes in morphometric parameters. *J Anat.* 1996;189:117–125.
35. Mabuchi F, Aihara M, Mackey MR, Lindsey JD, Weinreb RN. Regional optic nerve damage in experimental mouse glaucoma. *Invest Ophthalmol Vis Sci.* 2004;45:4352–4358.
36. Zhao X, Pearson KE, Stephan DA, Russell P. Effects of prostaglandin analogues on human ciliary muscle and trabecular meshwork cells. *Invest Ophthalmol Vis Sci.* 2003;44:1945–1952.
37. Zhou M, Li XM, Lavker RM. Transcriptional profiling of enriched populations of stem cells versus transient amplifying cells: a comparison of limbal and corneal epithelial basal cells. *J Biol Chem.* 2006;281:19600–19609.
38. Luna C, Li G, Liton PB, Epstein DL, Gonzalez P. Alterations in gene expression induced by cyclic mechanical stress in trabecular meshwork cells. *Mol Vis.* 2009;15:534–544.

39. Steele MR, Inman DM, Calkins DJ, Horner PJ, Vetter ML. Microarray analysis of retinal gene expression in the DBA/2J model of glaucoma. *Invest Ophthalmol Vis Sci.* 2006;47:977–985.
40. Shi X, Cui B, Wang Z, et al. Removal of Hsf4 leads to cataract development in mice through down-regulation of gamma S-crystallin and Bfsp expression. *BMC Mol Biol.* 2009;10:10.
41. Fuchshofer R, Stephan DA, Russell P, Tamm ER. Gene expression profiling of TGFbeta2- and/or BMP7-treated trabecular meshwork cells: identification of Smad7 as a critical inhibitor of TGF-beta2 signaling. *Exp Eye Res.* 2009;88:1020–1032.
42. Hiura K, Lim SS, Little SP, Lin S, Sato M. Differentiation dependent expression of tensin and cortactin in chicken osteoclasts. *Cell Motil Cytoskeleton.* 1995;30:272–284.
43. Tarone G, Cirillo D, Giancotti FG, Comoglio PM, Marchisio PC. Rous sarcoma virus-transformed fibroblasts adhere primarily at discrete protrusions of the ventral membrane called podosomes. *Exp Cell Res.* 1985;159:141–157.
44. Yamaguchi H, Lorenz M, Kempiak S, et al. Molecular mechanisms of invadopodium formation: the role of the N-WASP-Arp2/3 complex pathway and cofilin. *J Cell Biol.* 2005;168:441–452.
45. Abram CL, Seals DF, Pass I, et al. The adaptor protein fish associates with members of the ADAMs family and localizes to podosomes of Src-transformed cells. *J Biol Chem.* 2003;278:16844–16851.
46. Sato T, del Carmen Ovejero M, Hou P, et al. Identification of the membrane-type matrix metalloproteinase MT1-MMP in osteoclasts. *J Cell Sci.* 1997;110:589–596.
47. Gould DB, Smith RS, John SW. Anterior segment development relevant to glaucoma. *Int J Dev Biol.* 2004;48:1015–1029.
48. Sowden JC. Molecular and developmental mechanisms of anterior segment dysgenesis. *Eye* (*Lond*). 2007;21:1310–1318.
49. Gage PJ, Rhoades W, Prucka SK, Hjalt T. Fate maps of neural crest and mesoderm in the mammalian eye. *Invest Ophthalmol Vis Sci.* 2005;46:4200–4208.
50. Smith RS, Zabaleta A, Savinova OV, John SW. The mouse anterior chamber angle and trabecular meshwork develop without cell death. *BMC Dev Biol.* 2001;1:3.
51. Chang B, Smith RS, Peters M, et al. Haploinsufficient Bmp4 ocular phenotypes include anterior segment dysgenesis with elevated intraocular pressure. *BMC Genet.* 2001;2:18.
52. Kume T, Deng KY, Winfrey V, Gould DB, Walter MA, Hogan BL. The forkhead/winged helix gene Mf1 is disrupted in the pleiotropic mouse mutation congenital hydrocephalus. *Cell.* 1998;93:985–996.
53. Smith RS, Zabaleta A, Kume T, et al. Haploinsufficiency of the transcription factors FOXC1 and FOXC2 results in aberrant ocular development. *Hum Mol Genet.* 2000;9:1021–1032.
54. Weng J, Luo J, Cheng X, et al. Deletion of G protein-coupled receptor 48 leads to ocular anterior segment dysgenesis (ASD) through down-regulation of Pitx2. *Proc Natl Acad Sci U S A.* 2008;105:6081–6086.
55. Hjalt TA, Amendt BA, Murray JC. PITX2 regulates procollagen lysyl hydroxylase (PLOD) gene expression: implications for the pathology of Rieger syndrome. *J Cell Biol.* 2001;152:545–552.
56. Hassemer EL, Le Gall SM, Liegel R, et al. The waved with open eyelids (woe) locus is a hypomorphic mouse mutation in Adam17. *Genetics.* 2010;185:245–255.
57. Wordinger RJ, Fleenor DL, Hellberg PE, et al. Effects of TGF-beta2, BMP-4, and gremlin in the trabecular meshwork: implications for glaucoma. *Invest Ophthalmol Vis Sci.* 2007;48:1191–1200.
58. Fuchshofer R, Tamm ER. Modulation of extracellular matrix turnover in the trabecular meshwork. *Exp Eye Res.* 2009;88:683–688.
59. Alfandari D, Cousin H, Marsden M. Mechanism of xenopus cranial neural crest cell migration. *Cell Adh Migr.* 2010;4:553–560.
60. Faralli JA, Schwinn MK, Gonzalez JM, Jr., Filla MS, Peters DM. Functional properties of fibronectin in the trabecular meshwork. *Exp Eye Res.* 2009;88:689–693.
61. Hausman RE. Ocular extracellular matrices in development. *Prog Retin Eye Res.* 2007;26:162–188.
62. Crimaldi L, Courtneidge SA, Gimona M. Tks5 recruits AFAP-110, p190RhoGAP, and cortactin for podosome formation. *Exp Cell Res.* 2009;315:2581–2592.
63. Oikawa T, Itoh T, Takenawa T. Sequential signals toward podosome formation in NIH-src cells. *J Cell Biol.* 2008;182:157–169.
64. West-Mays JA, Pino G. Matrix Metalloproteinases as mediators of primary and secondary cataracts. *Expert Rev Ophthalmol.* 2007;2:931–938.
65. Wong TT, Sethi C, Daniels JT, Limb GA, Murphy G, Khaw PT. Matrix metalloproteinases in disease and repair processes in the anterior segment. *Surv Ophthalmol.* 2002;47:239–256.
66. Danias J, Lee KC, Zamora MF, et al. Quantitative analysis of retinal ganglion cell (RGC) loss in aging DBA/2NNia glaucomatous mice: comparison with RGC loss in aging C57/BL6 mice. *Invest Ophthalmol Vis Sci.* 2003;44:5151–5162.
67. Fujikawa K, Iwata T, Inoue K, et al. VAV2 and VAV3 as candidate disease genes for spontaneous glaucoma in mice and humans. *PLoS One* 5:e9050.
68. Harada T, Harada C, Nakamura K, et al. The potential role of glutamate transporters in the pathogenesis of normal tension glaucoma. *J Clin Invest.* 2007;117:1763–1770.
69. John SW, Smith RS, Savinova OV, et al. Essential iris atrophy, pigment dispersion, and glaucoma in DBA/2J mice. *Invest Ophthalmol Vis Sci.* 1998;39:951–962.
70. Mabuchi F, Lindsey JD, Aihara M, Mackey MR, Weinreb RN. Optic nerve damage in mice with a targeted type I collagen mutation. *Invest Ophthalmol Vis Sci.* 2004;45:1841–1845.
71. Zhou Y, Grinchuk O, Tomarev SI. Transgenic mice expressing the Tyr437His mutant of human myocilin protein develop glaucoma. *Invest Ophthalmol Vis Sci.* 2008;49:1932–1939.
72. Libby RT, Anderson MG, Pang IH, et al. Inherited glaucoma in DBA/2J mice: pertinent disease features for studying the neurodegeneration. *Vis Neurosci.* 2005;22:637–648.
73. McKinnon SJ, Schlamp CL, Nickells RW. Mouse models of retinal ganglion cell death and glaucoma. *Exp Eye Res.* 2009;88:816–824.